

# Effective-Lagrangian approach to $\gamma\gamma \rightarrow WW$ ; II: Results and comparison with $e^+e^- \rightarrow WW$

O. NACHTMANN <sup>1</sup>, F. NAGEL <sup>2</sup>, M. POSPISCHIL <sup>3</sup> AND A. UTERMANN <sup>4</sup>

*Institut für Theoretische Physik, Philosophenweg 16, D-69120 Heidelberg, Germany*

## Abstract

We present a study of anomalous electroweak gauge-boson couplings which can be measured in  $e^+e^-$  and  $\gamma\gamma$  collisions at a future linear collider like ILC. We consider the gauge-boson sector of a locally  $SU(2) \times U(1)$  invariant effective Lagrangian with ten dimension-six operators added to the Lagrangian of the Standard Model. These operators induce anomalous three- and four-gauge-boson couplings and an anomalous  $\gamma\gamma H$  coupling. We calculate the reachable sensitivity for the measurement of the anomalous couplings in  $\gamma\gamma \rightarrow WW$ . We compare these results with the reachable precision in the reaction  $e^+e^- \rightarrow WW$  on the one hand and with the bounds that one can get from high-precision observables in  $Z$  decays on the other hand. We show that one needs both the  $e^+e^-$  and the  $\gamma\gamma$  modes at an ILC to constrain the largest possible number of anomalous couplings and that the Giga- $Z$  mode offers the best sensitivity for certain anomalous couplings.

---

<sup>1</sup>email: O.Nachtmann@thphys.uni-heidelberg.de

<sup>2</sup>email: F.Nagel@thphys.uni-heidelberg.de

<sup>3</sup>Now at CNRS UPR 2191, 1 Avenue de la Terrasse, F-91198 Gif-sur-Yvette, France,  
email: Martin.Pospischil@iaf.cnrs-gif.fr

<sup>4</sup>email: A.Utermann@thphys.uni-heidelberg.de

# Contents

<b>1</b>	<b>Introduction</b>	<b>3</b>
<b>2</b>	<b>Preliminaries and present constraints</b>	<b>4</b>
<b>3</b>	<b>The process <math>\gamma\gamma \rightarrow WW \rightarrow 4</math> fermions</b>	<b>7</b>
3.1	Fixed photon energies . . . . .	7
3.2	Photons at a $\gamma\gamma$ collider . . . . .	9
3.3	Kinematics . . . . .	10
<b>4</b>	<b>Optimal observables</b>	<b>11</b>
<b>5</b>	<b>Results</b>	<b>14</b>
5.1	Anomalous couplings in $\gamma\gamma \rightarrow WW$ . . . . .	14
5.2	Comparison with $e^+e^- \rightarrow WW$ . . . . .	18
<b>6</b>	<b>Conclusions</b>	<b>20</b>
<b>A</b>	<b>Reconstruction ambiguities at a photon collider</b>	<b>22</b>

# 1 Introduction

A future linear electron-positron collider ILC with c.m. energies of 500 GeV and more offers excellent possibilities for high precision studies of the Standard Model (SM) of particle physics [1–4]. Particularly interesting is the electroweak gauge-boson sector where the SM couplings are fixed by the requirement of renormalisability. Deviations from the SM values for these gauge-boson couplings would be a clear sign of new physics. A comprehensive study of gauge-boson couplings is, therefore, highly desirable. To this end all options for the ILC, in particular  $e^+e^-$  and  $\gamma\gamma$  collisions, have to be considered.

In this paper we continue to explore and summarise the potential of a  $\gamma\gamma$  collider—especially in comparison to the  $e^+e^-$  mode—for constraining anomalous electroweak gauge-boson couplings  $h_i$  in an effective Lagrangian,

$$\mathcal{L}_{\text{eff}} = \mathcal{L}_0 + \mathcal{L}_2, \quad (1.1)$$

which respects the SM gauge symmetry group  $SU(3) \times SU(2) \times U(1)$  and contains only the SM fields. Here  $\mathcal{L}_0$  is the Lagrangian of the SM and

$$\begin{aligned} \mathcal{L}_2 = & \left( h_W O_W + h_{\tilde{W}} O_{\tilde{W}} + h_{\varphi W} O_{\varphi W} + h_{\varphi \tilde{W}} O_{\varphi \tilde{W}} + h_{\varphi B} O_{\varphi B} + h_{\varphi \tilde{B}} O_{\varphi \tilde{B}} \right. \\ & \left. + h_{WB} O_{WB} + h_{\tilde{W}\tilde{B}} O_{\tilde{W}\tilde{B}} + h_{\varphi}^{(1)} O_{\varphi}^{(1)} + h_{\varphi}^{(3)} O_{\varphi}^{(3)} \right) / v^2, \end{aligned} \quad (1.2)$$

contains all dimension-six operators  $O_i$  that either consist only of electroweak gauge-boson fields ( $W, B$  or  $\tilde{W}, \tilde{B}$  respectively) or that contain both gauge-boson fields and the SM-Higgs field ( $\varphi$ ). For the detailed definition of the operators in  $\mathcal{L}_0$  and  $\mathcal{L}_2$  see App. A in [5] and for a general discussion of operators with dimension higher than four see [6, 7] and references therein.

In (1.2)  $v \approx 246$  GeV denotes the vacuum expectation value of the SM-Higgs-boson field. The  $h_i$  are the anomalous couplings which are to be measured at the ILC. Since we introduce the factor  $1/v^2$  in  $\mathcal{L}_2$  the couplings  $h_i$  are dimensionless. From a measurement or from bounds of a  $h_i$  one can estimate a lower bound on the scale of new physics as

$$\Lambda = \frac{v}{\sqrt{|h_i| + \delta h_i}}. \quad (1.3)$$

Obviously, this approach is well suited to study effects of physics beyond the Standard Model (SM) at a future  $e^+e^-$  linear collider (LC) with a design like TESLA [1] or CLIC [2] in a model-independent way. A  $\gamma\gamma$  collider—where two high-energy photons are obtained through Compton backscattering of laser photons off high-energy electrons—extends the physics potential of a future LC substantially. Such a photon-collider option has been discussed for example for  $e^+e^-$  machines like TESLA [3] or CLIC [4].

It is particularly interesting to study the rich phenomenology induced by the Lagrangian (1.1) at a future LC both in the high-energy  $e^+e^-$  and  $\gamma\gamma$  modes, and in

the Giga- $Z$  mode. In a preceding work [8] the gauge-boson sector of such a Lagrangian and its implications for  $e^+e^- \rightarrow WW$  and for precision observables measured at the  $Z$  pole were studied. See also [9, 10] and references therein. In [5] we calculated the amplitudes for the process  $\gamma\gamma \rightarrow WW$  induced by the anomalous terms in the Lagrangian. Also the relation to other approaches [11–15] to anomalous couplings, like the use of form factors, was discussed, see [5].

In this work we study, in the framework of the Lagrangian (1.1), the process  $\gamma\gamma \rightarrow WW \rightarrow 4$  fermions. In the reaction  $\gamma\gamma \rightarrow WW$  anomalous contributions to the  $\gamma WW$ ,  $\gamma\gamma WW$  and  $\gamma\gamma H$  vertices can be studied. In particular we compare the results for the photon collider with those obtained in [8] for the reaction  $e^+e^- \rightarrow WW$  in order to see which anomalous couplings can be measured best in which collider mode.

Our paper is organised as follows: In Sect. 2 we summarise the results from [8] required here and give the bounds on the anomalous couplings that are calculated from present data. In Sect. 3 we review the differential cross section for the process  $\gamma\gamma \rightarrow WW$  with fixed c.m. energy of the two-photon system which was derived in the companion paper [5]. In Sect. 4 we review briefly the concept of the optimal observables. In Sect. 5 we use the optimal observables to calculate the reachable sensitivity to the anomalous couplings in  $\gamma\gamma \rightarrow WW$  at a future ILC. We compare these results with the sensitivity reachable in the  $e^+e^-$  mode both from  $e^+e^- \rightarrow WW$  and from  $Z$  production. Our conclusions are presented in Sect. 6.

## 2 Preliminaries and present constraints

In this section we summarise the results from [8] that are required in this paper. We also give the present bounds on the  $h_i$  as calculated in [8] from LEP and SLC results. The relation to other work on anomalous electroweak gauge-boson couplings [15–21] is discussed in [8].

After electroweak symmetry breaking some operators of  $\mathcal{L}_2$  lead to new three- and four-gauge-boson interactions, to  $\gamma\gamma H$  interactions, and some contribute to the diagonal and off-diagonal kinetic terms of the gauge bosons and of the Higgs boson as well as to the mass terms of the  $W$  and  $Z$  bosons. Thus one first has to identify the physical fields  $A$ ,  $Z$ ,  $W^\pm$  and  $H$ . As explained in [8] this requires a renormalisation of the  $W$ -boson and of the Higgs-boson fields. Furthermore, the kinetic matrix of the neutral gauge bosons has to be transformed into the unit matrix while keeping their mass matrix diagonal in order to obtain propagators of the standard form. The full Lagrangian (1.1) is then expressed in terms of the physical fields  $A$ ,  $Z$ ,  $W^\pm$  and  $H$ . In this procedure the neutral- and charged-current interactions are modified although no anomalous fermion-gauge-boson-interaction term is added explicitly. Therefore the Lagrangian (1.1) leads to a rich phenomenology to be probed at a future LC both in the high-energy  $e^+e^-$  and  $\gamma\gamma$  modes, and in the Giga- $Z$  mode.

We now recall the input parameter schemes introduced in [8]. In the Lagrangian

(1.1) the Higgs potential is that of the SM, cf. App. A of [5]. It contains the two parameters  $\mu^2$  and  $\lambda$ . They can be expressed in terms of the vacuum expectation value  $v$  and the Higgs-boson mass  $m_H$ . Then the effective Lagrangian contains the three electroweak parameters  $g$ ,  $g'$  and  $v$  where  $g$  and  $g'$  are the  $SU(2)$  and  $U(1)$  coupling constants. Apart from that it contains the mass  $m_H$  of the Higgs boson, nine fermion masses (neglecting neutrino masses), four parameters of the CKM matrix, and ten anomalous couplings  $h_i$ . In [8] two schemes,  $P_Z$  and  $P_W$ , were introduced that include, instead of  $g$ ,  $g'$  and  $v$ , the following electroweak parameters:

$$P_Z : \alpha(m_Z), G_F, m_Z; \quad P_W : \alpha(m_Z), G_F, m_W. \quad (2.1)$$

For the list of the other parameters, which are identical in both schemes, see Table 3 of [8]. Here  $\alpha(m_Z)$  is the fine-structure constant at the  $Z$  scale,  $G_F$  is the Fermi constant, and  $m_Z$  and  $m_W$  are the masses of the  $Z$  and the  $W$  bosons, respectively. All constants of the Lagrangian (1.1) can then be expressed in terms of one of the two parameter sets (2.1), the other SM parameters and the anomalous couplings  $h_i$ . Expressing the Lagrangian (1.1) in terms of the physical gauge-boson fields, the physical Higgs-boson field  $H$ , and the parameters of either  $P_Z$  or  $P_W$ ,  $\mathcal{L}_{\text{eff}}$  shows a non-linear dependence on the anomalous couplings  $h_i$ , although the original expression (1.1) is linear in the  $h_i$ . This non-linearity stems from the renormalisation of the  $W$  and the Higgs fields, and from the simultaneous diagonalisation in the neutral-gauge-boson sector as well as from expressing all constants in terms of the above input-parameter sets. We then expand the full Lagrangian (1.1) in the  $h_i$  and drop all terms of second or higher order in the  $h_i$ . That is, we keep only the leading order terms in  $(v/\Lambda)^2$ . Throughout this paper we consider the Lagrangian (1.1) after this reparametrisation and linearisation unless otherwise stated. Of course, the resulting expressions depend on whether we choose  $P_W$  or  $P_Z$  as parameter scheme.

As shown in [8] in linear order in the  $h_i$  the neutral-current boson-fermion interactions are modified by anomalous couplings in both schemes, the charged-current interactions are changed only in the scheme  $P_Z$  but in a universal way for all fermions. Furthermore, the  $W$ - ( $Z$ -)boson mass changes in the scheme  $P_Z$  ( $P_W$ ) in order  $h_i$ . Due to these modifications of the neutral- and charged-current interactions and of the boson-masses, bounds on the  $h_i$  from electroweak precision measurements at LEP and SLC can be derived as done in this framework in [8]. There the scheme  $P_Z$  is used for this purpose since  $m_Z$  is known more precisely than  $m_W$ . Without data from direct measurements of triple-gauge-boson couplings (TGCs) these bounds are of order  $10^{-3}$  for  $h_{WB}$  and  $h_\varphi^{(3)}$ . Moreover, a number of gauge-boson self-interactions and gauge-boson-Higgs-interactions are modified in order  $h_i$ , see Tab. 1. Note that we only list those vertices there that are relevant either in this paper or for the observables considered in [8]. Including direct measurements of TGCs at LEP2, one further  $CP$  conserving coupling ( $h_W$ ) and two  $CP$  violating couplings ( $h_{\tilde{W}}, h_{\tilde{W}B}$ ) are constrained in [8].

We now summarise the numerical results for these anomalous couplings calculated

	SM	$h_W$	$h_{\tilde{W}}$	$h_{\varphi W}$	$h_{\varphi\tilde{W}}$	$h_{\varphi B}$	$h_{\varphi\tilde{B}}$	$h_{WB}$	$h_{\tilde{W}B}$	$h_\varphi^{(1)}$	$h_\varphi^{(3)}$
$\gamma WW$	✓	✓	✓					✓	✓		
$ZWW$	✓	✓	✓					✓	✓		$P_Z$
$\gamma\gamma WW$	✓	✓	✓								
$\gamma\gamma H$				✓	✓	✓	✓	✓	✓		

Table 1: Contributions of the SM Lagrangian and of the anomalous operators (1.1) to different vertices in order  $O(h)$ . The coupling  $h_\varphi^{(3)}$  contributes to the  $ZWW$  vertex in the scheme  $P_Z$  but not in  $P_W$ .

in [8] from data obtained at LEP1, SLC, LEP2 and from further  $W$ -boson data. These bounds were derived in the scheme  $P_Z$ , see (2.1). The following numerical values for the input parameters were used [22, 23]:

$$1/\alpha(m_Z) = 128.95(5), \quad (2.2)$$

$$G_F = 1.16639(1) \times 10^{-5} \text{ GeV}^{-2}, \quad (2.3)$$

$$m_Z = 91.1876(21) \text{ GeV}, \quad (2.4)$$

and in the  $P_W$  scheme [22],

$$m_W = 80.423(39) \text{ GeV}. \quad (2.5)$$

Here as in [8], we use the following definition of the effective leptonic weak mixing angle:

$$s_{\text{eff}}^2 \equiv \sin^2 \theta_{\text{eff}}^{\text{lept}} = \frac{1}{4} \left( 1 - \frac{g_V^\ell}{g_A^\ell} \right), \quad (2.6)$$

where  $g_V^\ell$  and  $g_A^\ell$  are the vector and axial-vector neutral-current couplings of the leptons,  $\ell = e, \mu, \tau$ . In the  $P_Z$  scheme this quantity contains a particular linear combination of the couplings  $h_{WB}$  and  $h_\varphi^{(3)}$ , see (5.4) in [8]:

$$s_{\text{eff}}^2 = (s_{\text{eff}}^{\text{SM}})^2 (1 + 3.39 h_{WB} + 0.71 h_\varphi^{(3)}) . \quad (2.7)$$

A large number of  $Z$ -pole observables depends on the anomalous couplings only through  $s_{\text{eff}}^2$ , see table 16.1 of [23] and Sect. 5 of [8]. Thus the measured value of  $s_{\text{eff}}^2$  determines bounds on the linear combination of  $h_{WB}$  and  $h_\varphi^{(3)}$  occurring in (2.7). The total width of the  $Z$  boson,  $\Gamma_Z$ , the mass  $m_W$  and width  $\Gamma_W$  of the  $W$  boson depend on these two anomalous couplings in a different way. Therefore from the measured values of  $s_{\text{eff}}^2$ ,  $\Gamma_Z$ ,  $\sigma_{\text{had}}^0$ ,  $R_\ell^0$ ,  $m_W$  and  $\Gamma_W$  bounds on these two couplings individually are obtained in [8]. One further  $CP$  conserving coupling,  $h_W$ , enters the three-gauge-boson vertices  $\gamma WW$  and  $ZWW$  and therefore can be constrained when considering direct measurements of the TGCs. Altogether, from present data the three  $CP$  conserving couplings  $h_{WB}$ ,  $h_\varphi^{(3)}$  and  $h_W$  can be determined. We list the

$s_{\text{eff}}^2, \Gamma_Z, \sigma_{\text{had}}^0, R_\ell^0, m_W, \Gamma_W, \text{TGCs}$						
$m_H$	120 GeV	200 GeV	500 GeV	$\delta h \times 10^3$	W( $h$ )	
$h_W \times 10^3$	-62.4	-62.5	-62.8	36.3	1	-0.007 0.008
$h_{WB} \times 10^3$	-0.06	-0.22	-0.45	0.79		1 -0.88
$h_\varphi^{(3)} \times 10^3$	-1.15	-1.86	-3.79	2.39		

Table 2: Final results from [8] for  $CP$  conserving couplings in units of  $10^{-3}$  for a Higgs mass of 120 GeV, 200 GeV and 500 GeV respectively. The anomalous couplings are extracted from existing electroweak precision data for the observables listed in the first row. The errors  $\delta h$  and the correlations of the errors are independent of the Higgs mass within the given accuracy. The correlation matrix is given in the three right most columns.

corresponding results from [8] in Tab. 2. Since the SM predictions of these observables depend on the mass  $m_H$  of the Higgs boson, the bounds for the  $h_i$  are functions of  $m_H$ , too.

In addition, from the measurement of TGCs at LEP2 the following values for two  $CP$  violating couplings are obtained in [8],

$$h_{\bar{W}} = 0.068 \pm 0.081, \quad (2.8)$$

$$h_{\bar{W}B} = 0.033 \pm 0.084. \quad (2.9)$$

### 3 The process $\gamma\gamma \rightarrow WW \rightarrow 4$ fermions

#### 3.1 Fixed photon energies

In this section we review briefly the differential cross section for the process  $\gamma\gamma \rightarrow WW \rightarrow 4f$  in the presence of anomalous couplings. For more details see [5]. It is essential here to use the  $P_W$  scheme (2.1) since in the  $P_Z$  scheme the  $h_i$  would modify the  $W$  mass and therefore the kinematics of the reaction, which is highly inconvenient. The final-state fermions are leptons or quarks and we start with fixed photon energies. The case where the initial photons are not monochromatic but have Compton-energy spectra will be considered in the following section. Our notation for particle momenta and helicities is shown in Fig. 1. The production of the  $W$  bosons is described in the  $\gamma\gamma$  c.m. frame. Our coordinate axes are chosen such that the  $WW$ -boson production takes place in the  $x$ - $z$  plane, the photon momentum  $\mathbf{k}_1$  points in the positive  $z$ -direction and the unit vector in  $y$ -direction is given by  $\hat{\mathbf{e}}_y = (\mathbf{k}_1 \times \mathbf{k}_3)/|\mathbf{k}_1 \times \mathbf{k}_3|$ .

For unpolarised photons we obtain in the narrow-width approximation for the  $W$  bosons and considering all final-state fermions to be massless

$$\frac{d\sigma}{d\cos\Theta d\cos\vartheta d\varphi d\cos\bar{\vartheta} d\bar{\varphi}} = \frac{3\beta}{2^{13}\pi^3 s} B_{12} B_{34} \mathcal{P}_{\lambda'_3\lambda'_4}^{\lambda_3\lambda_4} \mathcal{D}_{\lambda'_3}^{\lambda_3} \bar{\mathcal{D}}_{\lambda'_4}^{\lambda_4}. \quad (3.1)$$

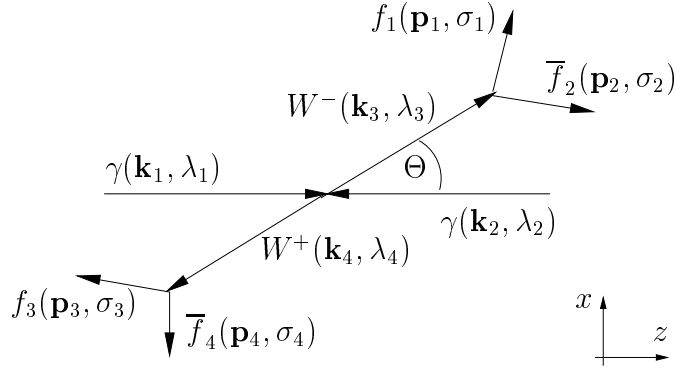


Figure 1: Conventions for particle momenta and helicities.

Here summation over repeated indices is implied and  $\beta = (1 - 4m_W^2/s)^{1/2}$  is the velocity of each  $W$  boson in the  $\gamma\gamma$  c.m. frame. The branching ratio for the decay  $W \rightarrow f_i \bar{f}_j$  is denoted by  $B_{ij}$ . The  $W$  helicity states are defined in the coordinate system shown in Fig. 1. For the definition of the polarisation vectors see App. C in [5]. The polar angle between the positive  $z$ -axis and the  $W^-$  momentum is denoted by  $\Theta$ . The cross section does not depend on the azimuthal angle of the  $W^-$  momentum due to rotational invariance. The respective frames for the decay tensors are defined by a rotation by  $\Theta$  about the  $y$ -axis of the frame in Fig. 1 such that the  $W^-$  ( $W^+$ ) momentum points in the new positive (negative)  $z$ -direction and a subsequent rotation-free boost into the c.m. system of the corresponding  $W$  boson. The spherical coordinates  $\vartheta, \varphi$  and  $\bar{\vartheta}, \bar{\varphi}$  are those of the  $f_1$ - and  $\bar{f}_4$ -momentum directions, respectively. The  $WW$ -production and  $W$ -decay tensors in (3.1) are given by

$$\mathcal{P}_{\lambda_3 \lambda_4}^{\lambda_1 \lambda_2}(\Theta) = \sum_{\lambda_1, \lambda_2} \mathcal{M}(\lambda_1, \lambda_2; \lambda_3, \lambda_4) \mathcal{M}^*(\lambda_1, \lambda_2; \lambda_3', \lambda_4'), \quad (3.2)$$

$$\mathcal{M}(\lambda_1, \lambda_2; \lambda_3, \lambda_4) \equiv \langle W^-(\mathbf{k}_3, \lambda_3) W^+(\mathbf{k}_4, \lambda_4) | \mathcal{T} | \gamma(\mathbf{k}_1, \lambda_1) \gamma(\mathbf{k}_2, \lambda_2) \rangle, \quad (3.3)$$

$$\mathcal{D}_{\lambda_3'}^{\lambda_3}(\vartheta, \varphi) = l_{\lambda_3} l_{\lambda_3'}^*, \quad (3.4)$$

$$\bar{\mathcal{D}}_{\lambda_4'}^{\lambda_4}(\bar{\vartheta}, \bar{\varphi}) = \bar{l}_{\lambda_4} \bar{l}_{\lambda_4'}^*, \quad (3.5)$$

where we have suppressed the phase-space variables on the right hand side. The production amplitudes  $\mathcal{M}$  and the functions occurring in the decay tensors are listed in App. D in [5].

To first order in the anomalous couplings the amplitudes  $\mathcal{M}$  are obtained from the SM diagrams, diagrams containing one anomalous triple- or quartic-gauge-boson vertex and the  $s$ -channel Higgs-boson exchange. The Feynman rules that are necessary to compute these diagrams are listed in App. B in [5]. This gives

$$\mathcal{M} = \mathcal{M}_{\text{SM}} + \sum_i h_i \mathcal{M}_i + O(h^2), \quad (3.6)$$



where all particle momenta and helicities are suppressed.  $\mathcal{M}_{\text{SM}}$  is the SM tree-level amplitude and  $i = W, \tilde{W}, \varphi W, \varphi \tilde{W}, \varphi B, \varphi \tilde{B}, WB, \tilde{W}B$ . The couplings  $h_\varphi^{(1)}$  and  $h_\varphi^{(3)}$  do not enter the amplitudes (3.6) to first order, since the related operators do not contribute to any anomalous gauge-boson vertex (see Tab. 1).

Since the couplings  $h_i, i = W, \tilde{W}, \varphi W, \varphi \tilde{W}, \varphi B, \varphi \tilde{B}, WB, \tilde{W}B$  contribute to the differential cross section, one could expect that these 8 couplings are measurable at a photon collider. But this is not the case since some amplitudes  $\mathcal{M}_i$  are related in a trivial way. We find the following relations between amplitudes, independently of helicities and momenta,

$$s_1^2 \mathcal{M}_{\varphi B} = c_1^2 \mathcal{M}_{\varphi W}, \quad (3.7)$$

$$s_1^2 \mathcal{M}_{\varphi \tilde{B}} = c_1^2 \mathcal{M}_{\varphi \tilde{W}}, \quad (3.8)$$

where

$$s_1^2 \equiv \frac{e^2}{4\sqrt{2}G_F m_W^2}, \quad c_1^2 \equiv 1 - s_1^2, \quad (3.9)$$

are combinations of input parameters in the  $P_W$  scheme. Hence the corresponding four anomalous couplings do not appear in the amplitudes in an independent way but only as linear combinations

$$h_{\varphi WB} \equiv s_1^2 h_{\varphi W} + c_1^2 h_{\varphi B}, \quad (3.10)$$

$$h_{\varphi \tilde{W} \tilde{B}} \equiv s_1^2 h_{\varphi \tilde{W}} + c_1^2 h_{\varphi \tilde{B}}. \quad (3.11)$$

We conclude that the process  $\gamma\gamma \rightarrow WW$  is sensitive to the anomalous couplings  $h_W, h_{\tilde{W}}, h_{\varphi WB}, h_{\varphi \tilde{W} \tilde{B}}, h_{WB}$  and  $h_{\tilde{W}B}$ . The couplings  $h_\varphi^{(1)}, h_\varphi^{(3)}$  and the orthogonal combinations to (3.10) and (3.11), that is

$$h'_{\varphi WB} = c_1^2 h_{\varphi W} - s_1^2 h_{\varphi B}, \quad (3.12)$$

$$h'_{\varphi \tilde{W} \tilde{B}} = c_1^2 h_{\varphi \tilde{W}} - s_1^2 h_{\varphi \tilde{B}}, \quad (3.13)$$

do not enter in the expressions for the amplitudes of  $\gamma\gamma \rightarrow WW$  due to (3.7) and (3.8).

## 3.2 Photons at a $\gamma\gamma$ collider

In the last section we discussed the differential cross section of the process  $\gamma\gamma \rightarrow WW \rightarrow 4f$  for fixed  $\gamma\gamma$  c.m. energy  $\sqrt{s}$ . However, at a real  $\gamma\gamma$  collider the photons do not have fixed energies in the laboratory system (LS) but they have a rather wide energy distribution. We now consider unpolarised photons whose energy is distributed according to a Compton spectrum [24]. This is still not completely realistic but good enough for our purposes.

We consider two beams of a collider where electrons of energy  $E_e$  (in the LS) scatter on laser photons of energy  $\omega$  to give high-energy photons by Compton scattering. According to (30a) in [24] the  $\gamma\gamma$  luminosity spectrum is given by

$$dL_{\gamma\gamma} = k^2 L_{ee} f\left(x, \frac{E_1}{E_e}\right) f\left(x, \frac{E_2}{E_e}\right) \frac{dE_1}{E_e} \frac{dE_2}{E_e}, \quad (3.14)$$

where  $E_1$  and  $E_2$  are the energies of the two photons in the LS,  $L_{ee}$  is the luminosity of the  $e^+e^-$  collider and  $k$  is the conversion factor for the  $\gamma$  production, see [24] for further details. The parameter  $x$  is given by

$$x = \frac{4 E_e \omega}{m_e^2} \cos^2 \frac{\alpha}{2}, \quad (3.15)$$

where  $m_e$  is the electron mass,  $\omega$  is the energy of the laser photons and  $\alpha$  is the angle between the incoming electron and the laser photon. Throughout this paper, we use  $x = 4.6$ . The energy spectrum of the scattered photons is, cf. (6a) in [24]:

$$f(x, y) = \left(\ln x + \frac{1}{2}\right)^{-1} \left[1 - y + \frac{1}{1-y} - \frac{4y}{x(1-y)} + \frac{4y^2}{x^2(1-y)^2}\right]. \quad (3.16)$$

Because we expressed the differential cross section in Sect. 3.1 as function of the squared  $\gamma\gamma$  c.m. energy  $s = 4E_1E_2$ , it is convenient to express the spectrum (3.14) in terms of  $s$  and  $E_1$  instead of  $E_1$  and  $E_2$ . Using (3.14), one gets,

$$dL_{\gamma\gamma} = \frac{k^2 L_{ee} \sqrt{s}}{2 E_e^2 E_1} f\left(x, \frac{E_1}{E_e}\right) f\left(x, \frac{s}{4 E_1 E_e}\right) dE_1 d\sqrt{s}. \quad (3.17)$$

For the unpolarised differential cross section of the process  $ee \rightarrow \gamma\gamma \rightarrow WW \rightarrow 4f$  induced by Compton backscattering we hence obtain:

$$\frac{d\sigma_{ee \rightarrow \gamma\gamma \rightarrow WW \rightarrow 4f}}{d\sqrt{s} dE_1 d\phi} = \frac{1}{L_{ee}} \frac{dL_{\gamma\gamma}}{d\sqrt{s} dE_1} \frac{d\sigma(\sqrt{s})}{d\phi} = \frac{k^2}{2 E_e^2} \tilde{S}, \quad (3.18)$$

$$\tilde{S} \equiv \frac{\sqrt{s}}{E_1} f\left(x, \frac{E_1}{E_e}\right) f\left(x, \frac{s}{4 E_1 E_e}\right) \frac{d\sigma(\sqrt{s})}{d\phi}, \quad (3.19)$$

where

$$\phi = (\Theta, \vartheta, \varphi, \bar{\vartheta}, \bar{\varphi}) \quad (3.20)$$

stands for the set of five phase space variables defined in Fig. 1 and  $d\sigma(\sqrt{s})/d\phi$  is the differential cross section (3.1) for fixed  $\gamma\gamma$  c.m. energy  $\sqrt{s}$ .

### 3.3 Kinematics

It is now easy to see that the final state in the reaction  $\gamma\gamma \rightarrow WW \rightarrow 4$  fermions at a photon collider is uniquely specified by the 7 variables

$$\chi \equiv (\sqrt{s}, E_1, \phi), \quad (3.21)$$

considering unpolarised photons and summing over the helicities of the final fermions. We would like to determine to which extent the variables  $\chi$  can be reconstructed in an experiment if we consider the case of one  $W$  decaying leptonically and one to a quark-antiquark pair,  $q\bar{q}$ , that is to two jets. We suppose that the jets are not tagged as  $q$  or  $\bar{q}$  jet and that, therefore, the (anti)quark cannot be associated to one of the two jets. We assume that the following variables can be measured:

$$\xi \equiv \left( k_{W,x}, k_{W,z}, \widehat{\mathbf{k}}_{\text{jet}}, \mathbf{k}_\ell \right). \quad (3.22)$$

Here  $k_{W,x}$  and  $k_{W,z}$  are the  $x$ - and  $z$ -components of the momentum in the LS of the  $W$  boson that decays into two jets. Furthermore,  $\widehat{\mathbf{k}}_{\text{jet}}$  is the momentum direction of one of the jets in the rest frame of this  $W$  and  $\mathbf{k}_\ell$  is the momentum of the charged lepton from the decay of the other  $W$  in the LS. In our coordinates we have  $k_{W,y} = 0$ , see Fig. 1. Thus 7 quantities are measurable on which the cross section depends in a non-trivial way. From counting of variables we therefore conclude that the full set of variables  $\chi$  may be reconstructible. However, there can be ambiguities, that is for events with certain measured kinematic variables  $\xi$  there may correspond two or more final states  $\chi_k$  with  $k = 1, 2, \dots$  that cannot be distinguished. Two different ambiguities occur in our reaction. The first one is due to the fact that the neutrino momentum cannot be directly measured, the second one occurs because the jet charges are not tagged. In App. A we take a closer look at these ambiguities.

## 4 Optimal observables

In Sect. 2 we saw that the operators  $O_{WB}$  and  $O_\varphi^{(3)}$  have an impact on electroweak precision observables measured at LEP and SLD, whereas the operators  $O_W, O_{\bar{W}}, O_{WB}$  and  $O_{\bar{W}\bar{B}}$  affect the  $W$ -pair production in  $e^+e^-$  collisions. According to the results of Sect. 3 we can constrain even more couplings in the process  $\gamma\gamma \rightarrow WW \rightarrow 4$  fermions, that is the linear combinations  $h_{\varphi WB}$  (3.10) and  $h_{\varphi \bar{W}\bar{B}}$  (3.11) which enter in the now accessible anomalous  $\gamma\gamma H$  vertex, see Tab. 1. To compute the maximum sensitivity of the normalised differential distribution to the anomalous couplings we use optimal observables [19, 20, 25]. This method has been applied to analyses of triple gauge couplings in the reaction  $e^+e^- \rightarrow WW$  in [18–20] which takes into account all statistical correlations of the errors on the couplings. We summarise below the general properties of optimal observables, see [26] for details.

In an experiment one measures the differential cross section

$$S(\xi) = d\sigma/d\xi, \quad (4.1)$$

where  $\xi$  denotes the set of all measured phase space variables. Expanding  $S$  in the anomalous couplings one can write

$$S(\xi) = S_0(\xi) + \sum_i S_i(\xi) h_i + O(h^2), \quad (4.2)$$

where  $S_0(\xi)$  is the tree-level cross section in the SM. One way to extract the anomalous couplings from the measured distribution (4.2) is to look for a suitable set of observables  $\mathcal{O}_i(\xi)$  whose expectation values

$$E[\mathcal{O}_i] = \frac{1}{\sigma} \int d\xi S(\xi) \mathcal{O}_i(\xi) \quad (4.3)$$

are sensitive to the dependence of  $S$  on the couplings  $h_i$ . Here, we will use the following observables,

$$\mathcal{O}_i(\xi) = \frac{S_i(\xi)}{S_0(\xi)}. \quad (4.4)$$

These observables are optimal in the sense that for  $h_i \rightarrow 0$  the errors on the couplings extracted from them are as small as they can be for a given probability distribution, see [19, 20, 26]. Using this set of observables the resulting covariance matrix is,

$$V(h) = \frac{1}{N} c^{-1} + O(h), \quad (4.5)$$

$$c_{ij} = \frac{\int d\xi (S_i(\xi) S_j(\xi))/S_0(\xi)}{\int d\xi S_0(\xi)} - \frac{\int d\xi S_i(\xi) \int d\xi S_j(\xi)}{(\int d\xi S_0(\xi))^2}. \quad (4.6)$$

Apart from being useful for actual experimental analyses, the observables (4.4) thus provide insight into the sensitivity that is at best attainable by *any* method, given a certain process—described by a differential cross section  $S(\xi)$ —and specified experimental conditions. We further note that phase space cuts, as well as detector efficiency and acceptance have no influence on the observables being "optimal" in the above sense, since their effects drop out in the ratio (4.4). This is not the case for detector resolution effects, but the observables (4.4) are still close to optimal if such effects do not significantly distort the differential distributions  $S_i$  and  $S_0$  (or tend to cancel in their ratio). To the extent that they are taken into account in the data analysis, none of these experimental effects will bias the estimators.

In the present work we use the method of optimal observables in the linear approximation valid for small anomalous couplings. But we emphasise that in [20] the method has been extended to the fully non-linear case where one makes no a priori assumptions on the size of anomalous couplings.

With the differential cross section (3.1) and the covariance matrix (4.5) in leading order of the anomalous couplings we have the basic ingredients at hand to calculate the sensitivities  $\delta h_i = \sqrt{V_{ii}}$ .

Now we construct the functions  $S_0(\xi)$  and  $S_i(\xi)$  needed for the optimal observables (4.4). The reconstruction ambiguities discussed in Sect. 3.3 and App. A introduce some slight complications. We start from a particular set of phase-space variables  $\chi$  that specifies the final state uniquely. In our case this set is given by (3.21). The differential cross section in terms of these variables is

$$T(\chi) \equiv d\sigma/d\chi. \quad (4.7)$$

The cross section for the measurable set of variables  $\xi$  (3.22), is then

$$S(\xi) = \int d\chi \delta(F(\chi) - \xi) T(\chi). \quad (4.8)$$

The function  $F$ , expressing the relation of  $\xi$  to  $\chi$ , may take the same value for different values of  $\chi$ , that is for a given  $\xi$  the equation

$$F(\chi) = \xi \quad (4.9)$$

may have several solutions  $\chi_k \equiv \chi_k(\xi)$  with  $k = 1, 2, \dots$ . In general, the number of solutions to (4.9) may vary with  $\xi$ . If  $\xi$  are the coordinates that can be measured of an event  $\chi$ , the set of final states  $\chi_k$  consists of  $\chi$  itself as well as all final states that cannot be distinguished from  $\chi$  by a measurement of  $\xi$ . Coming back to (4.8) we have

$$S(\xi) = \sum_k |J_k|^{-1} T(\chi_k(\xi)) \quad (4.10)$$

where

$$J_k \equiv \det \frac{\partial F}{\partial \chi}(\chi_k(\xi)) \quad (4.11)$$

is the Jacobian determinant taken at point  $\chi_k$ .

The cross section  $S(\xi)$  in (4.10) is to be used for the construction of the optimal observables according to (4.1) - (4.6). The sums which are generally occurring in (4.10) with the number of terms in the sum depending on  $\xi$  must be adequately treated in the integrations of (4.3) and (4.6). See [26] for the details.

We now apply these considerations to the reaction  $\gamma\gamma \rightarrow WW \rightarrow 4$  fermions. At a photon collider, the photons have a nontrivial energy spectrum as described in Sect. 3.2. The final state is specified uniquely by the variables  $\chi$ , see (3.21). If we assume that the variables  $\xi$  in (3.22) are measurable we obtain a two-fold ambiguity in the reconstruction of  $\xi$  for part of the phase space and a four-fold one for another part, see Sect. 3.3 and App. A. We must now calculate  $F(\chi)$  (4.9) and the Jacobian (4.11).

Suppose first that the  $W^+$  decays into leptons and the  $W^-$  hadronically. After performing the appropriate boosts and rotations between the reference frames defined in Sect. 3 and the LS we obtain

$$k_{W,x} = m_W \gamma \beta \sin \Theta, \quad (4.12)$$

$$k_{W,z} = m_W \gamma (b_- + b_+ \beta \cos \Theta), \quad (4.13)$$

$$k_{\ell,x} = \frac{m_W}{2} [\gamma(\cos \bar{\vartheta} - \beta) \sin \Theta + \sin \bar{\vartheta} \cos \bar{\varphi} \cos \Theta], \quad (4.14)$$

$$k_{\ell,y} = \frac{m_W}{2} \sin \bar{\vartheta} \sin \bar{\varphi}, \quad (4.15)$$

$$k_{\ell,z} = \frac{m_W}{2} [b_- \gamma(1 - \beta \cos \bar{\vartheta}) + b_+ \gamma(\cos \bar{\vartheta} - \beta) \cos \Theta - b_+ \sin \bar{\vartheta} \cos \bar{\varphi} \sin \Theta], \quad (4.16)$$

where

$$\gamma = \frac{\sqrt{s}}{2m_W}, \quad \beta = \sqrt{1 - 1/\gamma^2}, \quad b_{\pm} = \frac{4E_1^2 \pm s}{4E_1\sqrt{s}} = \frac{E_1 \pm E_2}{\sqrt{s}}. \quad (4.17)$$

Since the jet direction  $\widehat{\mathbf{k}}_{\text{jet}}$  is already defined in the  $W^-$  rest system, the relation to the angles of Fig. 1 is,

$$\widehat{\mathbf{k}}_{\text{jet}} = \begin{pmatrix} \sin \vartheta \cos \varphi \\ \sin \vartheta \sin \varphi \\ \cos \vartheta \end{pmatrix}. \quad (4.18)$$

Eqs. (4.12) to (4.16) together with (4.18) specify  $F(\chi)$  and the calculation of the Jacobian (4.11) is now straightforward. If  $W^-$  decays into leptons and  $W^+$  into quarks, we have to make the replacements

$$\begin{aligned} (\bar{\vartheta}, \bar{\varphi}) &\longrightarrow (\vartheta, \varphi) \\ \beta &\longrightarrow -\beta \end{aligned} \quad (4.19)$$

in (4.12) to (4.16) and in (4.18).

With this we have collected all tools needed for the evaluation of (4.10) and of the integrals in (4.3) and (4.6).

## 5 Results

### 5.1 Anomalous couplings in $\gamma\gamma \rightarrow WW$

We now give the sensitivity to the anomalous couplings in the reaction  $\gamma\gamma \rightarrow WW$  where we allow all couplings to deviate from zero simultaneously. These results are then compared to those obtained in [8] for  $e^+e^- \rightarrow WW$ . For the photon collider mode we consider the c.m. energies of the initial  $e^-e^-$  system as listed in the left-most column of Tab. 3. Energies of 500 GeV and 800 GeV are planned for the ILC and higher energies are supposed to be feasible at CLIC. The same energies are considered for the (standard)  $e^+e^-$  mode. The second column shows the integrated luminosities that we assume for the  $e^+e^-$  mode. Our calculations for the reaction  $\gamma\gamma \rightarrow WW$  are done for fixed c.m. energies  $\sqrt{s}$  of the two photon system as given in the third column and with a Compton spectrum for each photon as described in Sect 3.2. For the latter case the values for  $\sqrt{s}$  listed in the table roughly correspond to the maxima in the photon spectrum at the respective  $e^-e^-$  energies. For the integrated luminosity in the  $\gamma\gamma$  mode we use the approximation (cf. Sect. 4 of [3])

$$L_{\gamma\gamma} = \frac{1}{3}L_{ee}. \quad (5.1)$$

Using the input values (2.2) - (2.5) the total cross section for  $\gamma\gamma \rightarrow WW$  in the SM

$\sqrt{s_{ee}}$	$L_{ee}$	$\sqrt{s}$	$N/10^7$	$\frac{8}{27} N/10^7$
500 GeV	500 fb <sup>-1</sup>	400 GeV	1.5	0.44
800 GeV	1.0 ab <sup>-1</sup>	640 GeV	3.0	0.89
1.5 TeV	1.5 ab <sup>-1</sup>	1.2 TeV	4.5	1.3
3 TeV	3.0 ab <sup>-1</sup>	2.4 TeV	9.0	2.7

Table 3: From the left to the right, c.m. energy of the  $e^-e^-$  system (in the photon collider mode) or  $e^+e^-$  system, luminosity in the  $e^+e^-$  mode, c.m. energy  $\sqrt{s}$  of the  $\gamma\gamma$  system, total number of  $W$  pairs in units of  $10^7$  that are produced in  $\gamma\gamma \rightarrow WW$  and number of  $W$  pairs decaying semileptonically.

for unpolarised photon beams is  $\approx 90$  pb, almost constant in the energy range we consider. The number of produced  $W$  pairs is therefore

$$N \approx \frac{1}{3} L_{ee} 90 \text{ pb}, \quad (5.2)$$

which is given in the fourth column of Tab. 3. The number of events that is used for the statistical errors on the anomalous couplings is  $N$  times the branching ratio  $8/27$  for semileptonic decays of the  $W$  bosons, shown in the right-most column. In the optimal observables (4.4) any overall factor of the cross section, e.g. the conversion factor  $k$  in (3.18), cancels. Thus the total event rate appears in the covariance matrices of the anomalous couplings only as the statistical factor in the denominator of (4.5). The errors on the couplings for other total rates than those listed in Tab. 3 can therefore be easily calculated from the numbers listed below. We use the listed values for the total event rates  $N$  both for the case with fixed  $\gamma\gamma$  c.m. energy and for the case with the Compton spectrum.

We give the errors on the couplings in the presence of all other couplings. These errors are obtained from the diagonal elements of the covariance matrices of the anomalous couplings

$$\delta h_i = \sqrt{V(h)_{ii}}. \quad (5.3)$$

We also show the corresponding correlation matrices

$$W(h)_{ij} = \frac{V(h)_{ij}}{\sqrt{V(h)_{ii} V(h)_{jj}}}. \quad (5.4)$$

For these calculations we use the input values (2.2) - (2.5). For the Higgs mass we choose two different values namely 120 and 150 GeV. In Tab. 4 we show the sensitivities (5.3) and correlation matrices (5.4) using the covariance matrix (4.5) for various fixed  $\gamma\gamma$  c.m. energies  $\sqrt{s}$  and a Higgs mass of 120 GeV. In that case we have to deal only with the jet ambiguity, see App. A. We observe that there is no correlation between  $CP$ -violating and  $CP$ -conserving couplings. For  $\sqrt{s} = 400$  GeV all reachable errors are between  $2.3 \times 10^{-4}$  and  $1.2 \times 10^{-3}$ , except for  $h_{\bar{W}B}$  where it

is  $3.4 \times 10^{-3}$ . For all couplings except for  $h_{\tilde{W}B}$  and  $h_{\varphi\tilde{W}\tilde{B}}$  the sensitivity improves with rising energy, viz. a factor 1.6 to 3.9 with each energy step. This is in part a consequence of the increasing number  $N$  of produced  $W$  pairs entering the covariance matrix (4.5), see Tab. 3. Since the sensitivities (5.3) are proportional to  $1/\sqrt{N}$ , this will lead to an improvement of approximately 2.5 going from the smallest to the largest energies. We see that this is not the whole effect. Additionally, the sensitivities increase just because the impact of anomalous, higher-dimensional operators has to increase with rising energy.

In contrast, the errors on  $h_{\tilde{W}B}$  and  $h_{\varphi\tilde{W}\tilde{B}}$  increase slightly with rising energy. To understand this effect one has to take a closer look on the respective anomalous amplitudes in [5] in comparison to the SM amplitude. Let us just mention that the matrix (4.6) and the sensitivity would vanish if the optimal observable (4.4) were constant even if the absolute value of (4.4) would strongly increase. Hence the sensitivity can decrease even for increasing anomalous contribution, if the contribution of the corresponding dimension-six operator to the amplitude becomes proportional to the SM amplitude at high energies.

For the  $CP$  conserving couplings at 400 GeV most correlations are about 50 %. At higher energies only the correlation between  $h_{WB}$  and  $h_{\varphi WB}$  is large whereas all others in the  $CP$  conserving sector are about 20% or smaller. This is different for the  $CP$  violating couplings where all correlations are larger than about 60% at all energies. In particular, the correlation between  $h_{\tilde{W}B}$  and  $h_{\varphi\tilde{W}B}$  is -0.98 at 640 GeV and -1.0 at higher energies within the numerical errors. This can be understood as follows: For longitudinally polarised  $W$  bosons the three amplitudes  $\mathcal{M}_{\tilde{W}B}$ ,  $\mathcal{M}_{\varphi\tilde{W}}$  and  $\mathcal{M}_{\varphi\tilde{B}}$  show in the high-energy limit  $s \gg m_W^2$  the same dependence on the photon helicities and on the angle  $\Theta$ , see App. D in [5]. Since for transversely polarised  $W$  bosons the corresponding amplitudes are suppressed in this limit, the couplings  $h_{\varphi\tilde{W}\tilde{B}}$  and  $h_{\tilde{W}B}$  are highly correlated for  $s \gg m_W^2$ . Similar arguments explain the above mentioned energy behaviour of  $\delta h_{\tilde{W}B}$  and  $\delta h_{\varphi\tilde{W}\tilde{B}}$ .

To illustrate the dependence on the Higgs mass, we show in Tab. 5 sensitivities and correlation matrices calculated under the same conditions as those in Tab. 4. Only the Higgs mass is increased from 120 to 150 GeV. For the  $CP$ -conserving couplings only the coupling  $h_{\varphi WB}$  is influenced. For the smallest energy the sensitivity increases around 8% and is unchanged for the larger energies. The sensitivity on the  $CP$ -violating coupling  $h_{\tilde{W}B}$  increases around less than 1%. For the  $CP$ -violating coupling  $h_{\varphi\tilde{W}\tilde{B}}$  we observe the strongest dependence on the Higgs mass. The sensitivity increases between 13% at the smallest energy and around 1% at the largest energy. In conclusion we see that the dependence on the Higgs mass is small for the mass range 120-150 GeV. This is at present roughly the favoured mass window from direct searches and indirect evidence [27]. In the following we will focus on one certain value of the Higgs mass namely 120 GeV.

The results listed in Tab. 6 are similar to those in Tab. 4, but here the photons are distributed according to the Compton spectrum (CS). The relevant differential



<i>CP</i> -conserving couplings					<i>CP</i> -violating couplings				
400 GeV									
$h$	$\delta h$ $\times 10^3$	$W(h)$			$h$	$\delta h$ $\times 10^3$	$W(h)$		
		$h_W$	$h_{WB}$	$h_{\varphi WB}$			$h_{\tilde{W}}$	$h_{\tilde{W}B}$	$h_{\varphi\tilde{W}\tilde{B}}$
$h_W$	0.23	1	0.479	-0.256	$h_{\tilde{W}}$	0.31	1	0.690	-0.556
$h_{WB}$	0.89	0.479	1	-0.496	$h_{\tilde{W}B}$	3.41	0.690	1	-0.852
$h_{\varphi WB}$	1.16	-0.256	-0.496	1	$h_{\varphi\tilde{W}\tilde{B}}$	1.13	-0.556	-0.852	1
640 GeV									
$h$	$\delta h$ $\times 10^3$	$W(h)$			$h$	$\delta h$ $\times 10^3$	$W(h)$		
		$h_W$	$h_{WB}$	$h_{\varphi WB}$			$h_{\tilde{W}}$	$h_{\tilde{W}B}$	$h_{\varphi\tilde{W}\tilde{B}}$
$h_W$	0.083	1	0.332	-0.254	$h_{\tilde{W}}$	0.12	1	0.667	-0.654
$h_{WB}$	0.50	0.332	1	-0.648	$h_{\tilde{W}B}$	3.29	0.667	1	-0.979
$h_{\varphi WB}$	0.62	-0.254	-0.648	1	$h_{\varphi\tilde{W}\tilde{B}}$	1.26	-0.654	-0.979	1
1200 GeV									
$h$	$\delta h$ $\times 10^3$	$W(h)$			$h$	$\delta h$ $\times 10^3$	$W(h)$		
		$h_W$	$h_{WB}$	$h_{\varphi WB}$			$h_{\tilde{W}}$	$h_{\tilde{W}B}$	$h_{\varphi\tilde{W}\tilde{B}}$
$h_W$	0.033	1	0.178	-0.167	$h_{\tilde{W}}$	0.048	1	0.654	-0.655
$h_{WB}$	0.32	0.178	1	-0.792	$h_{\tilde{W}B}$	4.61	0.654	1	-0.998
$h_{\varphi WB}$	0.34	-0.167	-0.792	1	$h_{\varphi\tilde{W}\tilde{B}}$	1.88	-0.655	-0.998	1
2400 GeV									
$h$	$\delta h$ $\times 10^3$	$W(h)$			$h$	$\delta h$ $\times 10^3$	$W(h)$		
		$h_W$	$h_{WB}$	$h_{\varphi WB}$			$h_{\tilde{W}}$	$h_{\tilde{W}B}$	$h_{\varphi\tilde{W}\tilde{B}}$
$h_W$	0.011	1	0.086	-0.092	$h_{\tilde{W}}$	0.015	1	0.585	-0.586
$h_{WB}$	0.18	0.086	1	-0.907	$h_{\tilde{W}B}$	5.20	0.585	1	-1.000
$h_{\varphi WB}$	0.17	-0.092	-0.907	1	$h_{\varphi\tilde{W}\tilde{B}}$	2.17	-0.586	-1.000	1

Table 4: Errors  $\delta h$  in units of  $10^{-3}$  for the *CP* conserving (left) and *CP* violating couplings (right) in the presence of all other couplings and correlation matrices  $W(h)$  for a  $\gamma\gamma$  c.m. energy of  $\sqrt{s} = 400, 640, 1200$  and  $2400$  GeV with unpolarised beams. The mass of the Higgs boson is set to  $120$  GeV.

cross section is now given by (3.19). Furthermore, in addition to the jet ambiguity the neutrino ambiguity enters the calculation, see App. A. As we can see, if we compare the Tabs. 4 and 6, the results do not change so much. Due to the additional ambiguity, the errors for  $h_W$ ,  $h_{WB}$ ,  $h_{\varphi WB}$  and  $h_{\tilde{W}}$  are slightly higher. In contrast, the errors for  $h_{\tilde{W}B}$ ,  $h_{\varphi\tilde{W}\tilde{B}}$  are smaller except for the  $3000$  GeV case. This is easily understood: As already discussed above, the errors for these two couplings decrease with decreasing fixed  $\gamma\gamma$  c.m. energies. Taking the Compton spectrum into account, also lower energies with a better sensitivity will now enter the final result.

<i>CP</i> -conserving couplings					<i>CP</i> -violating couplings				
400 GeV									
$h$	$\delta h$ $\times 10^3$	$W(h)$			$h$	$\delta h$ $\times 10^3$	$W(h)$		
		$h_W$	$h_{WB}$	$h_{\varphi WB}$			$h_{\tilde{W}}$	$h_{\tilde{W}B}$	$h_{\varphi \tilde{W}\tilde{B}}$
$h_W$	0.23	1	0.477	-0.241	$h_{\tilde{W}}$	0.31	1	0.688	-0.536
$h_{WB}$	0.89	0.477	1	-0.466	$h_{\tilde{W}B}$	3.39	0.688	1	-0.829
$h_{\varphi WB}$	1.07	-0.241	-0.466	1	$h_{\varphi \tilde{W}\tilde{B}}$	0.99	-0.536	-0.829	1
640 GeV									
$h$	$\delta h$ $\times 10^3$	$W(h)$			$h$	$\delta h$ $\times 10^3$	$W(h)$		
		$h_W$	$h_{WB}$	$h_{\varphi WB}$			$h_{\tilde{W}}$	$h_{\tilde{W}B}$	$h_{\varphi \tilde{W}\tilde{B}}$
$h_W$	0.083	1	0.331	-0.250	$h_{\tilde{W}}$	0.12	1	0.671	-0.657
$h_{WB}$	0.50	0.331	1	-0.638	$h_{\tilde{W}B}$	3.33	0.671	1	-0.979
$h_{\varphi WB}$	0.60	-0.250	-0.638	1	$h_{\varphi \tilde{W}\tilde{B}}$	1.22	-0.657	-0.979	1
1200 GeV									
$h$	$\delta h$ $\times 10^3$	$W(h)$			$h$	$\delta h$ $\times 10^3$	$W(h)$		
		$h_W$	$h_{WB}$	$h_{\varphi WB}$			$h_{\tilde{W}}$	$h_{\tilde{W}B}$	$h_{\varphi \tilde{W}\tilde{B}}$
$h_W$	0.033	1	0.178	-0.167	$h_{\tilde{W}}$	0.048	1	0.655	-0.655
$h_{WB}$	0.32	0.178	1	-0.790	$h_{\tilde{W}B}$	4.61	0.655	1	-0.998
$h_{\varphi WB}$	0.34	-0.167	-0.790	1	$h_{\varphi \tilde{W}\tilde{B}}$	1.86	-0.655	-0.998	1
2400 GeV									
$h$	$\delta h$ $\times 10^3$	$W(h)$			$h$	$\delta h$ $\times 10^3$	$W(h)$		
		$h_W$	$h_{WB}$	$h_{\varphi WB}$			$h_{\tilde{W}}$	$h_{\tilde{W}B}$	$h_{\varphi \tilde{W}\tilde{B}}$
$h_W$	0.011	1	0.086	-0.092	$h_{\tilde{W}}$	0.015	1	0.583	-0.583
$h_{WB}$	0.18	0.086	1	-0.907	$h_{\tilde{W}B}$	5.15	0.583	1	-1.000
$h_{\varphi WB}$	0.17	-0.092	-0.907	1	$h_{\varphi \tilde{W}\tilde{B}}$	2.14	-0.583	-1.000	1

Table 5: Similar to Tab. 4 but with a Higgs mass of 150 GeV.

## 5.2 Comparison with $e^+e^- \rightarrow WW$

Finally, we would like to compare our results from Sect. 5.1 with those obtained for the reaction  $e^+e^- \rightarrow WW$  in [8]. Tab. 7 combines the sensitivities reachable at a  $e^+e^-$  collider [8] and a  $\gamma\gamma$  collider with the bounds that can be obtained using present data [8]. We see that the couplings  $h_{\varphi WB}$  and  $h_{\varphi \tilde{W}\tilde{B}}$  are only testable at a  $\gamma\gamma$  collider since only here the anomalous  $\gamma\gamma H$  vertex enters, see Tab. 1 and [5]. This already underlines the importance of the  $\gamma\gamma$  mode at a future LC. Concerning the reachable sensitivities for the couplings which are testable in both modes, the differences are quite small. Only for the couplings  $h_{WB}$  and  $h_{\tilde{W}B}$  one sees a clear tendency of the  $e^+e^-$  mode to give the better sensitivities.

On the left hand side of Tab. 7 we list the constraints [8] on the anomalous couplings that we can get from present data. These data cover precision observables and results of the direct measurement of triple gauge-couplings in  $e^+e^- \rightarrow WW$

<i>CP</i> -conserving couplings					<i>CP</i> -violating couplings				
500 GeV									
$h$	$\delta h$ $\times 10^3$	$W(h)$			$h$	$\delta h$ $\times 10^3$	$W(h)$		
		$h_W$	$h_{WB}$	$h_{\varphi WB}$			$h_{\tilde{W}}$	$h_{\tilde{W}B}$	$h_{\varphi\tilde{W}\tilde{B}}$
$h_W$	0.36	1	0.519	-0.120	$h_{\tilde{W}}$	0.46	1	0.630	-0.238
$h_{WB}$	1.08	0.519	1	-0.299	$h_{\tilde{W}B}$	3.17	0.630	1	-0.550
$h_{\varphi WB}$	1.17	-0.120	-0.299	1	$h_{\varphi\tilde{W}\tilde{B}}$	1.01	-0.238	-0.550	1
800 GeV									
$h$	$\delta h$ $\times 10^3$	$W(h)$			$h$	$\delta h$ $\times 10^3$	$W(h)$		
		$h_W$	$h_{WB}$	$h_{\varphi WB}$			$h_{\tilde{W}}$	$h_{\tilde{W}B}$	$h_{\varphi\tilde{W}\tilde{B}}$
$h_W$	0.13	1	0.407	-0.256	$h_{\tilde{W}}$	0.17	1	0.553	-0.491
$h_{WB}$	0.60	0.407	1	-0.547	$h_{\tilde{W}B}$	2.64	0.553	1	-0.904
$h_{\varphi WB}$	0.74	-0.256	-0.547	1	$h_{\varphi\tilde{W}\tilde{B}}$	0.97	-0.491	-0.904	1
1500 GeV									
$h$	$\delta h$ $\times 10^3$	$W(h)$			$h$	$\delta h$ $\times 10^3$	$W(h)$		
		$h_W$	$h_{WB}$	$h_{\varphi WB}$			$h_{\tilde{W}}$	$h_{\tilde{W}B}$	$h_{\varphi\tilde{W}\tilde{B}}$
$h_W$	0.050	1	0.265	-0.231	$h_{\tilde{W}}$	0.074	1	0.528	-0.525
$h_{WB}$	0.40	0.265	1	-0.741	$h_{\tilde{W}B}$	3.46	0.528	1	-0.988
$h_{\varphi WB}$	0.44	-0.231	-0.741	1	$h_{\varphi\tilde{W}\tilde{B}}$	1.39	-0.525	-0.988	1
3000 GeV									
$h$	$\delta h$ $\times 10^3$	$W(h)$			$h$	$\delta h$ $\times 10^3$	$W(h)$		
		$h_W$	$h_{WB}$	$h_{\varphi WB}$			$h_{\tilde{W}}$	$h_{\tilde{W}B}$	$h_{\varphi\tilde{W}\tilde{B}}$
$h_W$	0.016	1	0.146	-0.145	$h_{\tilde{W}}$	0.026	1	0.508	-0.509
$h_{WB}$	0.23	0.146	1	-0.881	$h_{\tilde{W}B}$	4.33	0.508	1	-0.999
$h_{\varphi WB}$	0.22	-0.145	-0.881	1	$h_{\varphi\tilde{W}\tilde{B}}$	1.80	-0.509	-0.999	1

Table 6: Errors  $\delta h_i$  and correlation matrices  $W(h)$  in units of  $10^{-3}$  for the *CP* conserving (left) and *CP* violating couplings (right) in the presence of all other couplings. We consider photons obtained through Compton backscattering off electrons with an *ee* c.m. energy of  $\sqrt{s_{ee}} = 500, 800, 1500$  and  $3000$  GeV. The mass of the Higgs boson is set to  $120$  GeV. The photons are supposed to be unpolarised and have an energy distributed according to a Compton spectrum, see Sect. 3.2. Since approximately 80% of the c.m. energy will be transferred into the  $\gamma\gamma$  system these results are comparable to the results from Tab. 4.

at LEP2. Surprisingly, we get good constraints on  $h_\varphi^{(3)}$  and  $h_{WB}$  from present high-precision observables, see Sect. 2 and [8]. The sensitivity for  $h_{WB}$  reachable in *W*-pair production at a future LC of the next generation is only of the same order as the present bound. Only at a LC with an even larger luminosity and energy like CLIC [2] we expect an improvement for this particular coupling. For the coupling  $h_\varphi^{(3)}$  we can not expect any improvements through *W*-pair production. The best way to

improve the knowledge about these two couplings at a LC would be to decrease the errors of the precision observables further. The Giga- $Z$  mode offers such a possibility. A measurement at the  $Z$  pole with an event rate that is about 100 times that of LEP1 should in essence reduce the errors  $\delta h_{WB}$  and  $\delta h_\varphi^{(3)}$  given in Tab. 7 by a factor of 10. The errors on the other couplings which are constrained only by the direct measurements of the triple gauge-couplings will improve significantly at a future LC.

## 6 Conclusions

We have presented an analysis of the phenomenology of the gauge-boson sector of an electroweak effective Lagrangian that is locally  $SU(2) \times U(1)$  invariant. In addition to the SM Lagrangian we included all ten dimension-six operators that are built either only from the gauge-boson fields of the SM or from the gauge-boson fields combined with the SM-Higgs field.

In a preceding work [8] the impact of these anomalous couplings onto observables from  $Z$  decays and  $W$  production at hadron and  $e^+e^-$  colliders were studied in this framework. For a large class of observables the anomalous effects only show up through a modified effective leptonic weak mixing angle. Other observables depend on the anomalous couplings in a different way and therefore lead to further constraints. From all data constraints on three  $CP$  conserving and two  $CP$  violating couplings were derived as reviewed in Sect. 2.

In the present paper we calculated the statistically best possible bounds on the anomalous couplings that can be obtained from  $\gamma\gamma \rightarrow WW$  at a photon collider by means of optimal observables. The couplings  $h_W, h_{WB}, h_{\tilde{W}}$  and  $h_{\tilde{W}B}$  can be measured both in  $\gamma\gamma \rightarrow WW$  and in  $e^+e^- \rightarrow WW$ . The sensitivity to these anomalous couplings achievable in the two reactions is similar. The couplings  $h_{\varphi WB}$  and  $h_{\varphi\tilde{W}\tilde{B}}$  can only be measured in  $\gamma\gamma \rightarrow WW$ .

We point out that one gets already today constraints for  $h_{WB}$  and  $h_\varphi^{(3)}$  from precision observables which are quite comparable with the sensitivity that one expects to reach in  $e^+e^- \rightarrow WW$  and  $\gamma\gamma \rightarrow WW$  at an ILC, see Sect. 5.2. Hence, we expect to get the best constraints for these two couplings by improving the accuracy of the precision observables, e.g. in the Giga- $Z$  mode of an ILC.

We summarise our findings. An ILC with  $e^+e^-$  collisions at  $\sqrt{s} = 500$  GeV will improve the sensitivity to the couplings  $h_W, h_{\tilde{W}}$  and  $h_{\tilde{W}B}$  compared to the present bounds by factors of about 140, 290 and 38, respectively. The Giga  $Z$  option will improve the bounds on  $h_{WB}$  and  $h_\varphi^{(3)}$  by about a factor of 10. Only the  $\gamma\gamma$  collider will make the study of the couplings  $h_{\varphi WB}$  and  $h_{\varphi\tilde{W}\tilde{B}}$  possible. The obtainable sensitivities are comparable to those for the other couplings from the  $e^+e^-$  mode. Three combinations out of the original ten anomalous couplings in (1.2), that is  $h_\varphi^{(1)}, h'_{\varphi WB}$  (3.12) and  $h'_{\varphi\tilde{W}\tilde{B}}$  (3.13) remain unmeasurable from the normalised event distributions of the reactions considered here.

	Constraints from LEP and SLD		Sensitivity at a LC					
			$e^+e^-$ mode		$\gamma\gamma$ mode fixed $\sqrt{s_{\gamma\gamma}}$		$\gamma\gamma$ mode with CS	
	$m_H$ [GeV]	$h_i$ $\times 10^3$	$\sqrt{s_{ee}}$ [GeV]	$\delta h_i$ $\times 10^3$	$\sqrt{s_{\gamma\gamma}}$ [GeV]	$\delta h_i$ $\times 10^3$	$\sqrt{s_{ee}}$ [GeV]	$\delta h_i$ $\times 10^3$
Measurable $CP$ -conserving couplings								
$h_W$	$-69 \pm 39$ Constraint from TGCs measurement at LEP 2		500	0.28	400	0.23	500	0.36
			800	0.12	640	0.083	800	0.13
					1200	0.033	1500	0.050
			3000	0.018	2400	0.011	3000	0.016
$h_{WB}$	120	$-0.06 \pm 0.79$	500	0.32	400	0.89	500	1.08
	200	$-0.22 \pm 0.79$	800	0.16	640	0.50	800	0.60
					1200	0.32	1500	0.40
	500	$-0.45 \pm 0.79$	3000	0.015	2400	0.18	3000	0.23
$h_{\varphi WB}$	Does not contribute		Does not contribute		400	1.16	500	1.17
					640	0.62	800	0.74
					1200	0.34	1500	0.44
					2400	0.17	3000	0.22
$h_{\varphi}^{(3)}$	120	$-1.15 \pm 2.39$	500	36.4	Does not contribute			
	200	$-1.86 \pm 2.39$	800	53.7				
	500	$-3.79 \pm 2.39$						
	3000	" $\infty$ "						
Measurable $CP$ -violating couplings								
$h_{\tilde{W}}$	$68 \pm 81$ Constraint from TGCs measurement at LEP 2		500	0.28	400	0.31	500	0.46
			800	0.12	640	0.12	800	0.17
					1200	0.048	1500	0.074
			3000	0.018	2400	0.015	3000	0.026
$h_{\tilde{W}B}$	$33 \pm 84$ Constraint from TGCs measurement at LEP 2		500	2.2	400	3.41	500	3.17
			800	1.4	640	3.29	800	2.64
					1200	4.61	1500	3.46
			3000	0.77	2400	5.20	3000	4.33
$h_{\varphi\tilde{W}\tilde{B}}$	Does not contribute		Does not contribute		400	1.13	500	1.01
					640	1.26	800	0.97
					1200	1.88	1500	1.39
					2400	2.17	3000	1.80

Table 7: The present constraints from LEP and SLD as calculated in [8] and reviewed in Sect. 2 and the expected sensitivities reachable in the different modes at a future LC are shown. We assume the integrated luminosities and the number of  $W$  pairs produced in  $\gamma\gamma \rightarrow WW$  as given in Tab. 3. For the calculation of the reachable sensitivity at a LC we choose a Higgs mass of 120 GeV.

A quantitative analysis of the sensitivities to anomalous couplings as presented here should help to decide how much total luminosity is required in each mode of a future ILC. As already explained in Sect. 1, our approach, using the effective Lagrangian (1.1) instead of form factors, is perfectly suited for a comprehensive study of all constraints on the  $h_i$  coming from different modes at an ILC and from high precision observables. We have seen that in any case the  $e^+e^-$  and the  $\gamma\gamma$  modes deliver complementary constraints on the anomalous couplings of the effective Lagrangian considered. Both modes as well as the Giga- $Z$  mode are indispensable for a comprehensive study of the gauge-boson sector at a future ILC.

## Acknowledgements

The authors are grateful to M. Diehl for reading a draft of this manuscript and to A. Denner and A. de Roeck for useful discussions. This work was supported by the German Bundesministerium für Bildung und Forschung, BMBF project no. 05HT4VHA/0, and the Deutsche Forschungsgemeinschaft through the Graduiertenkolleg “Physikalische Systeme mit vielen Freiheitsgraden”.

## A Reconstruction ambiguities at a photon collider

In Sect. 4 we discussed the consequences of reconstruction ambiguities for the calculation of the optimal observables (4.4) and the covariance matrix (4.5). Here we discuss the two ambiguities appearing at a photon collider, that is the one from the incomplete knowledge of the neutrino momentum and the one from no tag for the quark and antiquark jets.

The first ambiguity enters only if we consider a Compton spectrum for the photon energies. The lack of a direct measurement of the neutrino energy and momentum leads to a two-fold ambiguity in the identification of  $E_1$  and  $\sqrt{s}$ . Remember that the variables in (3.22) are the observable ones. Let  $\mathbf{k}_\nu$  be the neutrino momentum in the LS. Its component perpendicular to the beam axis is given by

$$\mathbf{k}_{\nu,\perp} = -\mathbf{k}_{\ell,\perp} - \mathbf{k}_{W,\perp}, \quad (\text{A.1})$$

with  $\mathbf{k}_{W,\perp} = (k_{W,x}, 0)$ . If  $\mathbf{k}_{\ell,\perp} \neq 0$  we have

$$k_{\nu,z} = \frac{1}{\mathbf{k}_{\ell,\perp}^2} (r k_{\ell,z} \pm g E_\ell), \quad E_\nu = \frac{1}{\mathbf{k}_{\ell,\perp}^2} (r E_\ell \pm g k_{\ell,z}), \quad (\text{A.2})$$

where

$$r = \frac{m_W^2}{2} + \mathbf{k}_{\ell,\perp} \cdot \mathbf{k}_{\nu,\perp}, \quad g = \sqrt{r^2 - \mathbf{k}_{\ell,\perp}^2 \mathbf{k}_{\nu,\perp}^2}. \quad (\text{A.3})$$

In (A.2) one has to *simultaneously* choose the upper *or* lower signs, i.e. there are two corresponding solutions, provided that both  $g$  and  $k_{\ell,z}$  are different from zero.

The energies of the photons in the LS are obtained from energy and momentum conservation:

$$E_1 + E_2 = E_W + E_\ell + E_\nu, \quad (\text{A.4})$$

$$E_1 - E_2 = k_{W,z} + k_{\ell,z} + k_{\nu,z}. \quad (\text{A.5})$$

For  $E_1$  we have

$$E_1 = \frac{1}{2}(E_W + E_\ell + E_\nu + k_{W,z} + k_{\ell,z} + k_{\nu,z}). \quad (\text{A.6})$$

One can easily check that in the case where there are two solutions (A.2) for  $k_{\nu,z}$  and  $E_\nu$ , these always lead to two different values for  $E_1$ . From (A.4) and (A.5) we obtain the squared  $\gamma\gamma$  c.m. energy

$$s = 4E_1E_2 = k_{W,x}^2 + \mathbf{k}_{\ell,\perp}^2 + \mathbf{k}_{\nu,\perp}^2 + 2(E_W E_\ell - k_{W,z} k_{\ell,z}) + 2(E_W + E_\ell)E_\nu + 2(k_{W,z} + k_{\ell,z})k_{\nu,z}. \quad (\text{A.7})$$

Inserting (A.2) into (A.7) we obtain in general two solutions for  $\sqrt{s}$ . In some regions of the parameter space one of these solutions must be discarded since the value of  $\sqrt{s}$  is unphysical. For some other cases where  $\mathbf{k}_{\ell,\perp}$  or  $g$  are zero the two solutions are identical. Because of these two reasons the two-fold neutrino ambiguity disappears in part of the parameter space.

The second ambiguity appears also in the case where the photon energies are fixed and arises since we supposed no identification of the charge of a jet. The relation between the measurable jet direction  $\hat{\mathbf{k}}_{\text{jet}}$  and the angles  $\vartheta$  and  $\varphi$  is given in (4.18). Since  $\hat{\mathbf{k}}_{\text{jet}}$  is already defined in the  $W^-$  ( $W^+$ ) rest frame, the second jet appearing in the hadronic decay of the  $W$  boson points in the opposite direction. Hence it is clear that the lack of jet-charge tagging leads to a two-fold ambiguity in the angles  $\vartheta, \varphi$ . Since the Jacobian  $J_k$  in (4.10) is trivial in this case one can handle this ambiguity basically through the restriction on one hemisphere in (4.18) to avoid the double counting of indistinguishable jets.

Due to the two described cases, the variables  $\chi$  (3.21) can be reconstructed only with a four-fold or a two-fold ambiguity depending on the input values for the measurable variables  $\xi$ .

## References

- [1] “TESLA Technical Design Report Part I: Executive Summary,” eds. F. Richard, J. R. Schneider, D. Trines and A. Wagner, DESY, Hamburg, 2001 [hep-ph/0106314];  
 “TESLA Technical Design Report Part III: Physics at an  $e^+e^-$  Linear Collider,” eds. R.-D. Heuer, D. Miller, F. Richard, P. M. Zerwas, DESY, Hamburg, 2001 [hep-ph/0106315].

- [2] J. R. Ellis, E. Keil and G. Rolandi, “Options for Future Colliders at CERN,” CERN-EP-98-03;  
J. P. Delahaye *et al.*, “CLIC—a Two-Beam Multi-TeV  $e^+e^-$  Linear Collider,” in: *Proc. of the 20th Intl. Linac Conference LINAC 2000* ed. Alexander W. Chao, eConf C000821, MO201 (2000) [physics/0008064];  
E. Accomando *et al.* [CLIC Physics Working Group Collaboration], “Physics at the CLIC multi-TeV linear collider,” CERN, Geneva, 2004, [arXiv:hep-ph/0412251].
- [3] “TESLA Technical Design Report, Part VI, Chapter 1: Photon Collider at TESLA,” B. Badelek *et al.*, DESY, Hamburg, 2001, [hep-ex/0108012].
- [4] H. Burkhardt and V. Telnov, “CLIC 3-TeV Photon Collider Option,” CERN-SL-2002-013-AP.
- [5] O. Nachtmann, F. Nagel, M. Pospischil and A. Utermann, *Eur. Phys. J. C* **45** (2006) 679 [hep-ph/0508132].
- [6] W. Buchmüller and D. Wyler, *Nucl. Phys. B* **268**, 621 (1986).
- [7] C. N. Leung, S. T. Love and S. Rao, *Z. Phys. C* **31**, 433 (1986).
- [8] O. Nachtmann, F. Nagel and M. Pospischil, *Eur. Phys. J. C* **42** (2005) 139 [arXiv:hep-ph/0404006].
- [9] K. Hagiwara, S. Ishihara, R. Szalapski and D. Zeppenfeld, *Phys. Lett. B* **283**, 353 (1992); K. Hagiwara, S. Ishihara, R. Szalapski and D. Zeppenfeld, *Phys. Rev. D* **48**, 2182 (1993).
- [10] K. Mönig, “Electroweak Gauge Theories and Alternative Theories at a Future Linear  $e^+e^-$  Collider,” hep-ph/0309021.
- [11] G. Tupper and M. A. Samuel, *Phys. Rev. D* **23** (1981) 1933;  
S. Y. Choi and F. Schrempp, *Phys. Lett. B* **272** (1991) 149;  
E. Yehudai, *Phys. Rev. D* **44** (1991) 3434; S. Y. Choi, K. Hagiwara and M. S. Baek, *Phys. Rev. D* **54** (1996) 6703 [hep-ph/9605334].
- [12] G. Bélanger and F. Boudjema, *Phys. Lett. B* **288** (1992) 210; M. Baillargeon, G. Bélanger and F. Boudjema, *Nucl. Phys. B* **500** (1997) 224 [hep-ph/9701372];  
G. Bélanger and G. Couture, *Phys. Rev. D* **49** (1994) 5720.
- [13] A. T. Banin, I. F. Ginzburg and I. P. Ivanov, *Phys. Rev. D* **59** (1999) 115001 [arXiv:hep-ph/9806515]; E. Gabrielli, V. A. Ilyin and B. Mele, *Phys. Rev. D* **60** (1999) 113005 [arXiv:hep-ph/9902362].



- [14] I. B. Marfin, V. A. Mossolov and T. V. Shishkina, “Anomalous quartic boson couplings via  $\gamma\gamma \rightarrow W^+W^-$  and  $\gamma\gamma \rightarrow W^+W^-Z$  at the TESLA kinematics,” hep-ph/0304250; A. Bredenstein, S. Dittmaier and M. Roth, Eur. Phys. J. C **36** (2004) 341 [hep-ph/0405169]; A. Bredenstein, S. Dittmaier and M. Roth, Eur. Phys. J. C **44** (2005) 27 [hep-ph/0506005].
- [15] I. Božović-Jelisavčić, K. Mönig and J. Šekarić, “Measurement of trilinear gauge couplings at a  $\gamma\gamma$  and  $e\gamma$  collider,” hep-ph/0210308.
- [16] K. J. F. Gaemers and G. J. Gounaris, Z. Phys. C **1**, 259 (1979);  
K. Hagiwara, R. D. Peccei, D. Zeppenfeld and K. Hikasa, Nucl. Phys. B **282**, 253 (1987).
- [17] I. Kuss and E. Nuss, Eur. Phys. J. C **4**, 641 (1998) [hep-ph/9706406].
- [18] M. Diehl, O. Nachtmann and F. Nagel, Eur. Phys. J. C **27**, 375 (2003) [hep-ph/0209229]; M. Diehl, O. Nachtmann and F. Nagel, Eur. Phys. J. C **32**, 17 (2003) [hep-ph/0306247].
- [19] M. Diehl and O. Nachtmann, Z. Phys. C **62**, 397 (1994).
- [20] M. Diehl and O. Nachtmann, Eur. Phys. J. C **1**, 177 (1998) [hep-ph/9702208].
- [21] F. A. Berends *et al.*, “Report of the working group on the measurement of triple gauge boson couplings,” J. Phys. G **24**, 405 (1998) [hep-ph/9709413];  
T. Abe *et al.* [American Linear Collider Working Group Collaboration], in *Proc. of the APS/DPF/DPB Summer Study on the Future of Particle Physics (Snowmass 2001)* ed. N. Graf, SLAC-R-570 *Resource book for Snowmass 2001, 30 Jun - 21 Jul 2001, Snowmass, Colorado*; W. Menges, “A study of charged current triple gauge couplings at TESLA,” LC-PHSM-2001-022.
- [22] K. Hagiwara *et al.* [Particle Data Group Collaboration], Phys. Rev. D **66**, 010001 (2002).
- [23] D. Abbaneo *et al.*, “A combination of preliminary electroweak measurements and constraints on the standard model,” arXiv:hep-ex/0212036.
- [24] I. F. Ginzburg, G. L. Kotkin, V. G. Serbo and V. I. Telnov, Nucl. Instrum. Meth. **205** (1983) 47.
- [25] D. Atwood and A. Soni, Phys. Rev. D **45**, 2405 (1992); M. Davier, L. Duflot, F. Le Diberder and A. Roug e, Phys. Lett. B **306**, 411 (1993).
- [26] O. Nachtmann and F. Nagel, Eur. Phys. J. C **40** (2005) 497 [hep-ph/0407224].
- [27] S. Eidelman *et al.* [Particle Data Group Collaboration], Phys. Lett. B **592** (2004) 1.